Ann. Geophys., 32, 507–518, 2014
www.ann-geophys.net/32/507/2014/
doi:10.5194/angeo-32-507-2014

Annales Geophysicae
Open Access

Resonant scattering of energetic electrons in the plasmasphere by monotonic whistler-mode waves artificially generated by ionospheric modification

S. S. Chang[1,2], B. B. Ni[1,2], J. Bortnik[2], C. Zhou[1], Z. Y. Zhao[1], J. X. Li[3], and X. D. Gu[1]

[1]Department of Space Physics, School of Electronic Information, Wuhan University, Wuhan, Hubei 430072, China
[2]Department of Atmospheric and Oceanic Sciecnes, University of California, Los Angeles, Los Angeles, California 90095-1565, USA
[3]Institute of Space Physics and Applied Technology, Peking University, Beijing 100871, China

Correspondence to: S. S. Chang (whu.css1108@gmail.com)

Received: 19 October 2013 – Revised: 20 January 2014 – Accepted: 4 April 2014 – Published: 21 May 2014

Abstract. Modulated high-frequency (HF) heating of the ionosphere provides a feasible means of artificially generating extremely low-frequency (ELF)/very low-frequency (VLF) whistler waves, which can leak into the inner magnetosphere and contribute to resonant interactions with high-energy electrons in the plasmasphere. By ray tracing the magnetospheric propagation of ELF/VLF emissions artificially generated at low-invariant latitudes, we evaluate the relativistic electron resonant energies along the ray paths and show that propagating artificial ELF/VLF waves can resonate with electrons from ~ 100 keV to ~ 10 MeV. We further implement test particle simulations to investigate the effects of resonant scattering of energetic electrons due to triggered monotonic/single-frequency ELF/VLF waves. The results indicate that within the period of a resonance timescale, changes in electron pitch angle and kinetic energy are stochastic, and the overall effect is cumulative, that is, the changes averaged over all test electrons increase monotonically with time. The localized rates of wave-induced pitch-angle scattering and momentum diffusion in the plasmasphere are analyzed in detail for artificially generated ELF/VLF whistlers with an observable in situ amplitude of ~ 10 pT. While the local momentum diffusion of relativistic electrons is small, with a rate of $< 10^{-7}\,s^{-1}$, the local pitch-angle scattering can be intense near the loss cone with a rate of $\sim 10^{-4}\,s^{-1}$. Our investigation further supports the feasibility of artificial triggering of ELF/VLF whistler waves for removal of high-energy electrons at lower L shells within the plasmasphere. Moreover, our test particle simulation results show quantitatively good agreement with quasi-linear diffusion coefficients, confirming the applicability of both methods to evaluate the resonant diffusion effect of artificial generated ELF/VLF whistlers.

Keywords. Space plasma physics (wave–particle interactions)

1 Introduction

Generation of extremely low-frequency (ELF)/very low-frequency (VLF) waves by modulated heating of the D region ionosphere in the presence of naturally forming ionospheric currents is by now a well-established technique (e.g., Ferraro et al., 1982; Barr and Stubbe, 1991; Inan et al., 2004; Platino et al., 2006; Piddyachiy et al., 2008; and references therein). Periodic heating of the ionospheric region with a high-frequency (HF) transmitter modulates the conductivity of the region and, in turn, modulates these naturally forming (and pre-existing) currents, constituting what amounts to a giant radiating antenna at ~ 60–100 km altitude. The natural current system can be the auroral electrojet modulated by High-Power Auroral Stimulation (HIPAS) or High-Frequency Active Auroral Research Program (HAARP) heating facilities (Inan et al., 2004; Platino et al., 2006; Piddyachiy et al., 2008), or the equatorial dynamo current modulated by the Arecibo heating facilities (Ferraro et al., 1982).

A number of observations, both ground-based and spaceborne, of ELF/VLF waves triggered in this manner have been carried out. Those observational results indicate that some of these artificial ELF/VLF waves generated by ionospheric modulation can propagate directly upwards and penetrate through the ionosphere into the overlying magnetosphere (James et al., 1984), and others propagate within the Earth–ionosphere waveguide and leak up progressively with each reflection off the ionosphere (Bell et al., 2004; Platino et al., 2006). The wave intensity detected by the ground-based receiver or by the spacecraft instrument is generally at a magnitude of a few pT. In contrast, DEMETER (Detection of Electromagnetic Emissions Transmitted from Earthquake Regions) spacecraft observations of ELF/VLF signals generated by the recently upgraded HAARP facility have revealed a very high intensity ($\boldsymbol{E} \simeq 350\,\mu\mathrm{V\,m^{-1}}$, $\boldsymbol{B} \simeq 20\,\mathrm{pT}$) within a narrow cylindrical of $\sim$ 10–20 km radius (Piddyachiy et al., 2008)

Propagation of artificial ELF/VLF waves in the magnetosphere can potentially resonantly interact with the high-energy electrons in the plasmasphere. The acceleration and loss of energetic electrons has been of increasing interest to magnetospheric physicists over the past decades (e.g., Thorne, 2010, and references therein). Since wave–particle interactions are believed to play an essential role in controlling electron dynamics, a variety of plasmas waves, such as whistler-mode chorus, plasmaspheric hiss, electromagnetic ion cyclotron (EMIC) waves, magnetosonic wave, and lightning-generated whistlers are studied intensively to assess their effects on electron diffusion as a result of resonant wave–particle interactions (e.g., Abel and Thorne, 1998a, b; Summers et al., 2007a, b; Summers and Ni, 2008; Thorne, 2010; Mourenas et al., 2013; Shprits et al., 2013). Being aware of the potential of controlling energetic electron lifetimes using artificial ELF/VLF waves, Inan at al. (2003) provided estimates of the potential effects of a satellite-based ELF/VLF transmitter at a few kHz operating at the magnetic equatorial plane of $L = 2$ and concluded that cyclotron resonances with the artificially injected whistler-mode waves can significantly reduce the lifetime of energetic electrons in the inner radiation belt. To estimate the wave-induced pitch-angle scattering rates, Inan et al. (2003) followed the quasi-linear formulae of Lyons (1974) and Albert (1999) in the limit of vanishing width of the frequency and wave-normal angle distribution. Later, Kulkarni et al. (2008) followed the methodology of Bortnik et al. (2006a, b), which assumed that the wave–particle interactions are linear and transformed the wave-induced pitch angle changes to precipitating flux using a novel convolution method. They modeled the potential electron precipitation signatures induced by hypothetical VLF transmitters distributed broadly in geomagnetic latitude and operating at four frequencies (i.e., 10 kHz, 20 kHz, 30 kHz, and 40 kHz). Their results indicated that the VLF sources located at 15° to 55° can induce the most $>$ 100 keV precipitation and induced precipitation increases as the operating frequency decreases.

While the linear or quasi-linear theory of resonant wave–particle interactions can operate feasibly for linear or stochastic particle-scattering processes in association with small amplitude waves over certain frequency band with random phase, test particle simulations can provide for monotonic/single-frequency waves more reasonable evaluations of the wave–particle interaction process and of the changes of particle pitch angle and energy in detail (e.g., Dysthe, 1971; Bortnik and Thorne, 2010; Tao and Bortnik, 2010; Tao et al., 2011; Zheng et al., 2012, 2013). As an important complement, here we perform comprehensive test particle simulations to investigate the potential scattering effects of artificial, single-frequency ELF/VLF whistlers on high-energy electrons in the plasmasphere. Use of test particle simulations can help us acquire the details of pitch angle and energy changes when resonances occur between electrons and artificial ELF/VLF whistlers and quantify the corresponding rates of pitch-angle scattering and energy diffusion. In addition, the present study mainly concentrates on the triggering of ELF/VLF emissions by HF heating at the invariant latitudes mapped inside the plasmasphere, which thus can provide specific, instructive information for ionospheric heating experiments in the low-latitude region other than in higher-latitude region (e.g., the HAARP location) as of the potential contribution of artificial ELF/VLF whistler waves for controlled precipitation of high-energy electrons in near-Earth environment.

Aiming to establish a feasible connection between ELF/VLF wave generation due to ground-based modulated ionospheric modification and resonant wave–particle interactions in space, this study is organized as follows. Section 2 presents our ray tracing results of ELF/VLF emissions by assuming that these waves at different single frequencies are already generated by modulated HF heating experiments at low latitudes. The propagation properties of artificially triggered ELF/VLF waves are intensively explored for a number of initial launch latitudes where the heater nominally operates. In Sect. 3, the resonance conditions between artificial monotonic ELF/VLF waves and energetic electrons in the plasmasphere are investigated along the ray paths modeled in Sect. 2. This can provide us with the exact information about the energy of electrons in resonance with generated ELF/VLF whistlers and its dependence on wave propagation location and resonance harmonics. The results of test particle simulations at $L = 3$ inside the plasmasphere are shown in Sect. 4. The details of multiple electron energy and pitch-angle variation with time due to resonant interactions with waves are presented to evaluate the average effect of wave-induced localized pitch-angle scattering and momentum diffusion. The computed local diffusion coefficients based on test particle simulations are also quantitatively compared with the quasi-linear diffusion rates obtained using the UCLA Full Diffusion Code (FDC) (Ni et al., 2008; Shprits and Ni, 2009). In

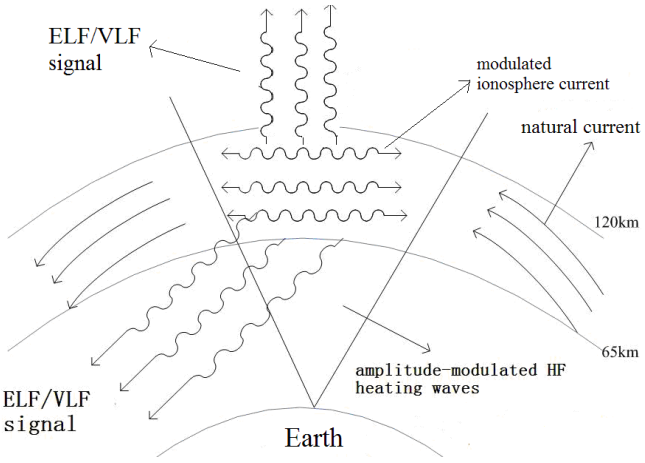

Figure 1. Schematic showing the generation of ELF/VLF whistler waves by modulated HF heating of the ionosphere and their subsequent propagation.

Sect. 5, we discuss our results and the limitation of this study for future improvements. We summarize our conclusions in Sect. 6.

2 Ray tracing simulations of ELF/VLF waves generated by modulated HF heating of the ionosphere

As shown schematically in Fig. 1, when ELF/VLF waves are generated as a result of periodic modulation of the ionospheric currents by HF heating (Ferraro et al., 1982; Barr and Stubbe, 1991; Inan et al., 2004; Platino et al., 2006; Piddyachiy et al., 2008), some waves propagate directly upwards and others propagate within the Earth–ionosphere waveguide and leak up progressively with each reflection off the ionosphere (James et al., 1984; Inan et al., 2004; Bell et al., 2004; Platino et al., 2006; Piddyachiy et al., 2008). Subsequently, these leaked waves propagate outwards and encounter energetic electrons that can potentially undergo resonant wave–particle interactions. When the ELF/VLF waves reach the higher ionosphere, at the altitudes ≥ 120 km in this study, the geometric optics theory is valid, and numerical ray tracing simulations are a good technique to determine the ray paths of the whistler-mode artificial waves. Actually, previous studies have performed ray tracing to simulate the propagation path of artificial ELF/VLF signals generated by heating the ionosphere (James et al., 1984; Platino et al., 2006) or by ground-based or satellite-based ELF/VLF transmitters (Inan et al., 2003; Kulkarni et al., 2008), and magnetospherically reflecting whistlers induced by lightning (Bortnik et al., 2003, 2006a, b; Bortnik, 2005). The ray tracing program used for the present computations is similar to that described by Inan and Bell (1977) (including the geomagnetic filed and electron density model). Their cold plasma diffusion equilibrium model is also used for calculation of reflective index in the following sections of the present paper.

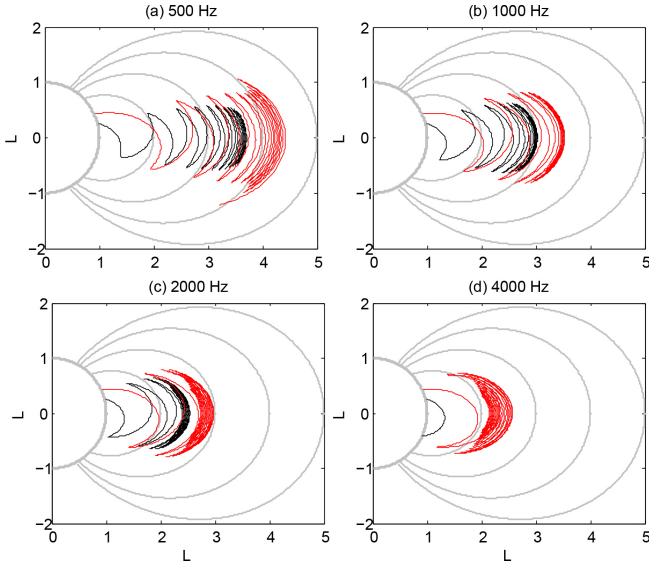

Figure 2. Ray paths of waves launched from two latitudes of 15° (black curves) and 25° (red curves), at four wave frequencies: **(a)** 500 Hz, **(b)** 1 kHz, **(c)** 2 kHz, and **(d)** 4 kHz. The initial altitude is 120 km and δ is 0° for all cases. Here δ is the angle between the wave-normal vector and the radial vector.

Here, we select waves at four frequencies, 0.5, 1, 2, and 4 kHz, which are within the general frequency band associated with the HF modulated heating facilities (e.g., Ferraro et al., 1982; Barr and Stubbe, 1991; Platino et al., 2006; Piddyachiy et al., 2008). We also perform the ray tracing starting at two latitudes, 15° (black curves) and 25° (red curves), focusing on ELF/VLF whistler wave triggering at low latitudes (Ferraro et al., 1982). By doing so, we can investigate the dependence of wave propagation path on both wave frequency and initial launch latitude. In addition, the initial angle between the wave normal and the radial vector is set as 0° for all ray tracing runs, due to the large value of the refractive index for these whistler waves in the ionosphere, compared to the free space (e.g., Bortnik et al., 2006a, b).

The simulation results are shown in Fig. 2. We can see that the artificial ELF/VLF waves, once entering into the magnetosphere, bounce back and forth between the Southern and Northern hemispheres, propagate outwards, and finally settle down at certain higher L shell, which is consistent with the results of Inan et al. (2003) and Bortnik (2005). Figure 2 also shows that the frequency and initial launch latitude strongly affects the details of ray path. Waves at low frequency or launched at a higher latitude can propagate further outwards, thus reaching higher L shells with a broader spatial coverage (e.g., Bortnik et al., 2003). This feature is clearly illustrated by the separation between the two sets of color-coded ray paths.

The use of ray tracing is to theoretically confirm that ELF/VLF waves, once triggered by modulated HF heating of the ionosphere, can leak into the inner magnetosphere for

potential resonant interactions with energetic electron. The study of the dependence of the wave trajectory on the frequency and launch latitude can provide specific, instructive information for ionospheric heating experiments in the low-latitude region as of the potential contribution of artificial ELF/VLF whistler waves for controlled precipitation of high-energy electrons in the near-Earth environment. Moreover, ray tracing simulations help provide the detailed information of wave properties including the wave-normal angle, which can be very useful in the quantitative investigation on resonant interactions between waves and electrons.

3 Resonance condition for interactions of artificially triggered ELF/VLF waves with plasmaspheric electrons

With the information of wave properties obtained by ray tracing and background magnetic field and electron density available, we can evaluate electron resonant energies and investigate whether a resonance can occur between a given wave frequency and electron energy, following the relativistic resonance condition

$$\omega - k_{//} v_{//} = \frac{N|\Omega_e|}{\gamma}, N = 0, \pm 1, \pm 2, \ldots, \quad (1)$$

where ω is the wave frequency, $k_{//} = k\cos\psi$ is the wave number component parallel to the ambient magnetic field with $k = \mu\omega/c$ as the total wave number and ψ as the wave-normal angle, $v_{//} = v\cos\alpha$ is the particle velocity component parallel to ambient magnetic field with α as the pitch angle, N is the resonance harmonic number, Ω_e is the electron gyrofrequency, and γ is the Lorentz factor given by $\gamma = (1-\beta^2)^{-1/2}$ with $\beta = v/c$. After a number of mathematical manipulations, Eq. (6) can change into

$$\omega - \mu\omega\beta\cos\psi\cos\alpha = N|\Omega_e|\sqrt{1-\beta^2}. \quad (2)$$

As seen from Eq. (2), β can be resolved for any pair of (α, N), once the wave frequency, the wave-normal angle, and the ambient density and magnetic field are specified. Subsequently, we can obtain the energy of particles resonating with the waves at given frequency by $\boldsymbol{E} = ((1-\beta^2)^{-1/2} - 1)mc^2$.

As an example, here we concentrate on the case of 1000 Hz with the initial launch latitude of 15°, shown as the black curve in Fig. 2b, to explore the resonant condition for interactions of triggered ELF/VLF waves with electrons in the inner magnetosphere. The wave-normal angle obtained by ray tracing is shown as black curve (labeled on the right) in each panel of Fig. 3, showing a fluctuated variation between ∼ 80° and 100° featured by multiple crossings of 90° associated with magnetospheric reflections. Along the ray path (within 9 s), we compute the resonant energies of electrons for a range of equatorial pitch angle from 1° ∼ 89° with these highly oblique waves. We also investigate four resonance harmonics, i.e., $N = -1, 0, 1,$ and 2, which should be

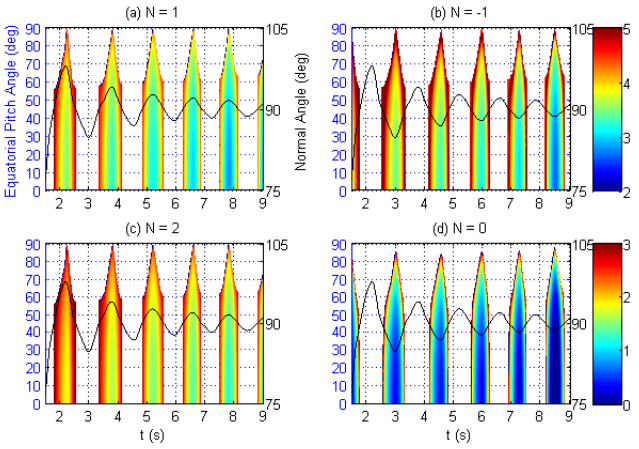

Figure 3. Electron resonant energies for various pitch angles along the ray path (within 1.5 s–9 s) of 1 kHz waves launched from a latitude of 15° for four resonance harmonics: **(a)** $N = 1$, **(b)** $N = -1$, **(c)** $N = 2$, and **(d)** $N = 0$. The curve of wave-normal angle along the ray path is shown in black. Here, **(a)–(c)** are indicated by the top color bar (10^2–10^5 keV) and **(d)** are indicated by the bottom color bar (1–10^3 keV).

the dominant resonances for interactions with whistler-mode waves (e.g., Shprits and Ni, 2009; Ni et al., 2013). Note that $|N| > 2$ can also occur for resonances with very high-energy electrons, while their contributions are relatively small compared to the resonance harmonics considered in this study. In addition, the cyclotron resonant energies (Fig. 3a, b and c) are color-coded by the top color bar ranging from 10^2 keV to 10^5 keV, while the Landau resonant energies (Fig. 3d) are color-coded by the bottom color bar of 10^0–10^3 keV. It is clear that resonant electron energies for the cyclotron resonances are much higher than those for the Landau resonance.

As shown in Fig. 3, resonances between energetic electrons at various equatorial pitch angles and artificial ELF/VLF whistlers at 1 kHz have a number of interesting features along the ray path. First, the resonance for a fixed harmonic does not occur continuously along the ray path. Specifically, resonances for harmonics $N = 1$ and 2 occur when wave-normal angle is above 90°, and the other two resonance harmonics occur when the normal angle is below 90°. Note that we have assumed that the electrons move in one direction with respect to the positive z axis. Second, resonant electron energy increases sharply (up to 100 MeV) as the artificially triggered waves approach the magnetospheric reflection points, indicated by the approach of the wave-normal angle to 90°. The major reason is that high wave-normal angle ∼ 90° reduces $k_{//}$ substantially and consequently elevates the resonant energy. In contrast, resonant energies are relatively low (∼ 100 keV to ∼ MeV) at the magnetic equator where the wave-normal angle deviates considerably from 90°. Third, resonant electron energy shows a strong dependence on the order of resonance harmonic. Resonant energy is highest for

$N = 2$, always above MeV as shown by the Fig. 3c, and becomes lower for $N = -1, 1$, and 0. Unlike the cyclotron resonances, the Landau resonance ($N = 0$) seems to occur only for $\boldsymbol{E} <\sim 10$ keV electrons along the major trajectory of artificial ELF/VLF waves, as shown in Fig. 3d, while for larger pitch angle the resonance can occur at higher electron energies. Also note that, as the waves propagate outward, the resonance energy becomes gradually smaller at the equator, while the normal angle progressively approaches 90°. An explanation can be that during outward propagation to higher-L shell, smaller ambient magnetic field and electron density increases the refractive index and subsequently the value of $k_{//}$, which lowers the resonant electron energies for all resonance harmonics.

4 Test particle simulation results

To investigate in detail the effect of resonant interactions between artificially generated ELF/VLF whistler waves and energetic electrons in the plasmasphere, instead of adopting the quasi-linear theory that assumes a broadband and incoherent wave field with small wave amplitude, we perform test particle simulations to evaluate the electron diffusion driven by HF heating triggered waves at a single frequency. This approach is different than the method of Inan et al. (2003). Our study is also different from Kulkarni et al. (2008) that modeled the potential electron precipitation signatures produced by ground-based single-frequency (10–40 kHz) VLF sources based on the methodology of Bortnik et al. (2006a, b). As an important complement, here we perform comprehensive test particle simulations to acquire the details of pitch angle and energy changes when resonances occur between high-energy electrons and artificial (< 5 kHz) ELF/VLF whistlers and quantify corresponding rates of pitch-angle scattering and energy diffusion. The major focus is directed towards tracing the temporal variations of electron pitch angle and kinetic energy under the impact from localized artificial ELF/VLF waves at $L = 3$. Thus we use a homogeneous background magnetic field $\boldsymbol{B}_0 = \boldsymbol{B}_0\boldsymbol{e}_z$ with $\boldsymbol{B}_0$ as the dipole field strength and $\boldsymbol{e}_z$ as unit vector. The discussion of this simple assumption is deferred to Sect. 5. Then electron trajectories are calculated by solving the general, the fully relativistic Lorentz equation:

$$\frac{\mathrm{d}\boldsymbol{x}}{\mathrm{d}t} = \frac{\boldsymbol{p}}{\gamma m}, \tag{3}$$

$$\frac{\mathrm{d}\boldsymbol{p}}{\mathrm{d}t} = q\left[\boldsymbol{E}_\mathrm{w} + \frac{\boldsymbol{p}}{\gamma m} \times (\boldsymbol{B}_\mathrm{w} + \boldsymbol{B}_0)\right], \tag{4}$$

where $\boldsymbol{p}$ is the electron momentum, m and q is the electron mass and charge, respectively. Note that the sign of the charge is contained in q. The artificial ELF/VLF emissions are whistler-mode waves, and the wave magnetic and electric fields with wave-normal vector $\boldsymbol{k} = k\,(\sin\psi, 0, \cos\psi)$ are given by

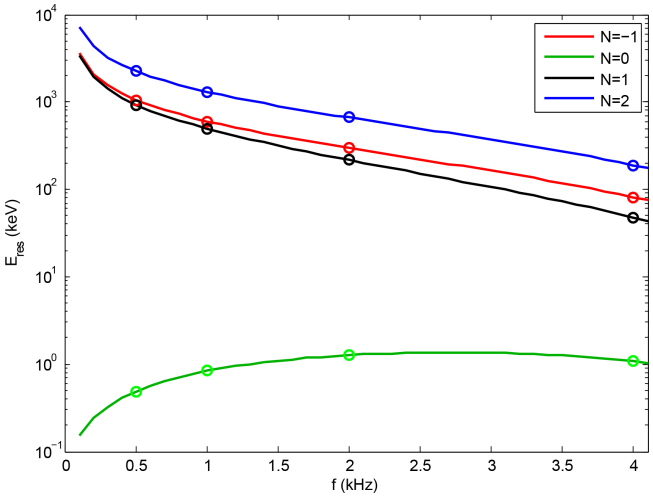

Figure 4. Electron resonant energies as a function of wave frequency at the magnetic equator of $L = 3$ for four resonance harmonics when the electron pitch angle is fixed as 30°. The red spots mark the resonant energies for four specified wave frequencies (i.e., 0.5, 1, 2, and 4 kHz.)

$$\boldsymbol{B}_w = \boldsymbol{e}_x \boldsymbol{B}_x^\mathrm{w} \cos\Phi - \boldsymbol{e}_y \boldsymbol{B}_y^\mathrm{w} \sin\Phi + \boldsymbol{e}_z \boldsymbol{B}_z^\mathrm{w} \cos\Phi, \tag{5}$$

$$\boldsymbol{E}_w = -\boldsymbol{e}_x \boldsymbol{E}_x^\mathrm{w} \sin\Phi - \boldsymbol{e}_y \boldsymbol{E}_y^\mathrm{w} \cos\Phi - \boldsymbol{e}_z \boldsymbol{E}_z^\mathrm{w} \sin\Phi, \tag{6}$$

where $\boldsymbol{e}_z$ is along the direction of background magnetic field, and $\boldsymbol{e}_x$ and $\boldsymbol{e}_y$ are the unit vectors within the equatorial plane, completing the right-hand coordinate system. Wave field $\boldsymbol{B}_i^\mathrm{w}$ and $\boldsymbol{E}_i^\mathrm{w}$ can be calculate when $\boldsymbol{B}_y^\mathrm{w}$ is given (Tao and Bortnik, 2010). $\Phi \equiv \int \boldsymbol{k} \cdot \mathrm{d}\boldsymbol{r} - \int \omega \mathrm{d}t$ is the wave phase angle. Following Tao et al. (2011), we use an ensemble of 200 electrons with identical values of initial pitch angle and energy, but having initial gyro-phases (the angle between $v_\perp$ and $\boldsymbol{e}_x$) distributed uniformly between 0 and 2π to investigate the ensemble and the averaged effect of wave-induced resonance. Considering the ray tracing results shown in Figs. 2 and 3, we select the location of $L = 3$ inside the plasmasphere and the wave-normal angle as 100° for the $N = 1$, 2 resonances and as 80° for $N = -1$, 0 resonances in the following calculations, which is different from Inan et al. (1984) that only considered wave propagation along the magnetic field lines and Inan et al. (2003) that set the wave-normal angle as 45°. In addition, according to the previous in situ observations of HF heater-generated ELF/VLF whistler waves (Platino et al., 2006; Piddyachiy et al., 2008), $\boldsymbol{B}_y^\mathrm{w}$ is taken to be nominally 10 pT for all the following simulations.

With all these parameters available at the equator of $L = 3$, we compute the resonant electron energies as a function of wave frequency (100 Hz–4 kHz) for the resonance harmonics $N = -1$, 0, 1, and 2, the results of which are shown in Fig. 4 for fixed pitch angle of 30°. The red spots mark the resonant electron energies corresponding to four wave frequencies

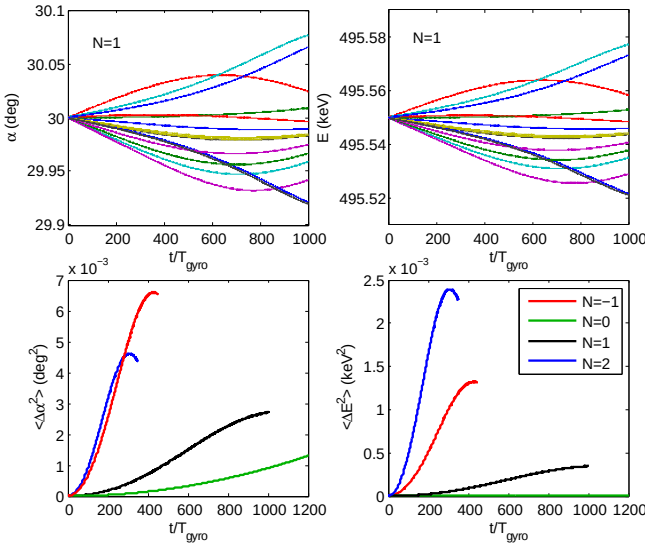

Figure 5. Results of resonant diffusion of an ensemble of electrons having the same initial pitch angle 30° and different energies to resonate with artificial waves at 1 kHz for four resonance harmonics. Top: changes of pitch angle (left) and kinetic energy (right) of 15 randomly selected electrons for the $N = 1$ resonance. Bottom: changes of $\Delta\alpha^2$ (left) and $\Delta \boldsymbol{E}^2$ (right) averaged over all 200 electrons for four resonance harmonics, $N = -1$, 0, 1, and 2. Note that initial electron energy varies with resonance harmonic to satisfy the resonance condition and consequently $T_{\rm gyro}$ also varies with resonance harmonic.

(i.e., 500, 1000, 2000, and 4000 Hz), the ray paths of which are illustrated in Fig. 2. It is apparent that resonant electron energy decreases with increasing whistler wave frequency for the cyclotron resonances ($N = -1$, 1, and 2) but increases with wave frequency for the Landau resonance.

We first concentrate on the cases of waves at a fixed frequency of 1000 Hz. Based on the Eqs. (3)–(6), we simulate the trajectories of 200 electrons with the same initial pitch angle (fixed as 30°) and the same initial energy in each run. The initial electron energy is selected to satisfy the resonance condition 2) for interactions with 1 kHz whistler waves at the equator of $L = 3$. As shown in Fig. 4, the initial electron kinetic energy for test particle simulations is taken as 601.58 keV, 836.91 eV, 495.55 keV, and 1.3084 MeV for the resonance harmonic $N = -1$, 0, 1, and 2, respectively. The test particle simulation results are presented in Fig. 5. As an example, the top panels show the temporal changes of pitch angle and kinetic energy for 15 randomly selected test electrons in the ambient magnetic field combined with the electric and magnetic field of artificial whistler waves at 1 kHz. The initial electron energy is chosen as 495.55 keV to satisfy the resonance condition for $N = 1$. When looking at the variations of pitch angle and kinetic energy separately, during the simulation some electrons increase monotonically, some decrease monotonically, and some increase initially and then decrease, indicating a stochastic process consistent with the results of Tao et al. (2011). Specifically, within 1000 gyroperiods (~ 0.062 s), change in electron pitch angle varies between $\pm 0.1°$ and change in electron kinetic energy varies between ± 0.03 keV. The change magnitudes (i.e., $\Delta\alpha = \alpha - \alpha_0$ and $\Delta \boldsymbol{E} = \boldsymbol{E} - \boldsymbol{E}_0$) are also stochastic for the 200 test electrons, resulting from random initial gyro-phases. The bottom panels of Fig. 5 show the magnitudes of $\Delta\alpha^2$ and $\Delta \boldsymbol{E}^2$ averaged over all 200 electrons, color coded for the four resonance harmonics $N = -1$, 0, 1, and 2. Note that to obtain the optimal illustration of resonant wave–particle interactions, while retaining the initial pitch angle at 30°, initial electron kinetic energies are different to satisfy the resonance conditions for the four resonance harmonics, as given above. Since the resonance can not last forever, we define the duration from the beginning to the point where the diffusion effect becomes negligibly weak as "resonance timescale". Within the period of resonance timescale, $\Delta\alpha^2$ and $\Delta \boldsymbol{E}^2$ due to wave-induced resonance increases monotonically with time. As shown in the plots, $\langle \Delta\alpha^2 \rangle$ or $\langle \Delta \boldsymbol{E}^2 \rangle$ (where $\langle \ldots \rangle$ denotes averaging over all electrons) increases with time and demonstrates a reasonably linear profile for the four resonance harmonics. For resonant interactions with 1 kHz whistler-mode waves around the magnetic equator of $L = 3$, the resonance timescales are respectively 0.030 s for 601.58 keV electrons at the $N = -1$ resonance, 0.063 s for 836.91 eV electrons at the Landau resonance, 0.068 s for 495.55 keV at the $N = 1$ resonance, and 0.034 s for 1.3084 MeV at the $N = 2$ resonance. A more detailed discussion of the "resonance timescale" is presented in Sect. 5.

Our results indicate an electron diffusion process resulting from resonant interactions with single-frequency whistler waves triggered by HF ionospheric heating. It is necessary and also straightforward to quantify the test particle diffusion coefficients using $D^{\rm TP}_{\alpha\alpha} = \langle \Delta\alpha^2 \rangle / 2\Delta t$ and $D^{\rm TP}_{\rm EE} = \langle \Delta \boldsymbol{E}^2 \rangle / 2\Delta t$ (e.g., Tao et al., 2011). Specifically, test particle diffusion coefficients are obtained by fitting in terms of $y = A + Bt$ to the temporal curves $\Delta\alpha^2$ and $\Delta \boldsymbol{E}^2$ with $D^{\rm TP}_{\alpha\alpha}(D^{\rm TP}_{\rm EE}) = \boldsymbol{B}/2$. The computed localized pitch-angle diffusion coefficients ($D^{\rm TP}_{\alpha\alpha}$) are $3.17 \times 10^{-6}\,{\rm s}^{-1}$, $5.20 \times 10^{-7}\,{\rm s}^{-1}$, $6.67 \times 10^{-7}\,{\rm s}^{-1}$, $2.03 \times 10^{-6}\,{\rm s}^{-1}$, and localized momentum diffusion rates ($D^{\rm TP}_{\rm EE}$) are $2.08 \times 10^{-9}\,{\rm s}^{-1}$, $4.37 \times 10^{-12}\,{\rm s}^{-1}$, $2.79 \times 10^{-10}\,{\rm s}^{-1}$, $3.46 \times 10^{-9}\,{\rm s}^{-1}$, for 601.58 keV ($N = -1$), 836.91 eV ($N = 0$), 495.55 keV ($N = 1$), and 1.3084 MeV ($N = 2$), respectively. While the local diffusion coefficients for $N = -1$ and $N = 2$ are larger, these comparisons are less meaningful since the resonant electron energies for the four harmonics are quite different. The histograms showing the number distribution of 200 test electrons with respect to relative change in pitch angle and energy, that is, $\Delta\alpha$ (left panels) and $\Delta \boldsymbol{E}$ (right panels) are presented in Fig. 6. On one hand, the 200 test electrons as a whole exhibit stochastic behaviors in terms of random changes in electron pitch angle and energy. On the other hand, the details of test electron distribution are quite different with respect to each

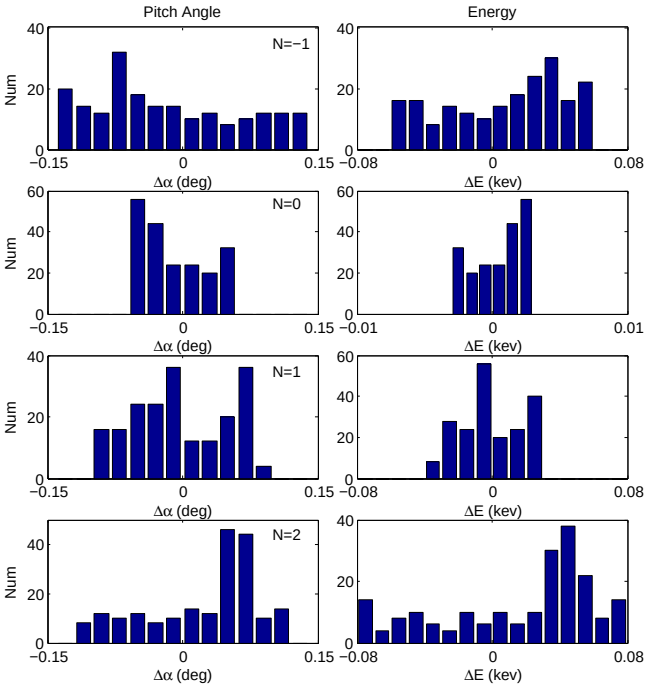

Figure 6. Corresponding to the bottom panels of Fig. 5, histograms showing the number distribution of 200 test electrons with respect to relative change in pitch angle and energy, that is, $\Delta\alpha$ (left panels) and $\Delta \boldsymbol{E}$ (right panels), for the resonance harmonics $N = -1$, 0, 1, and 2.

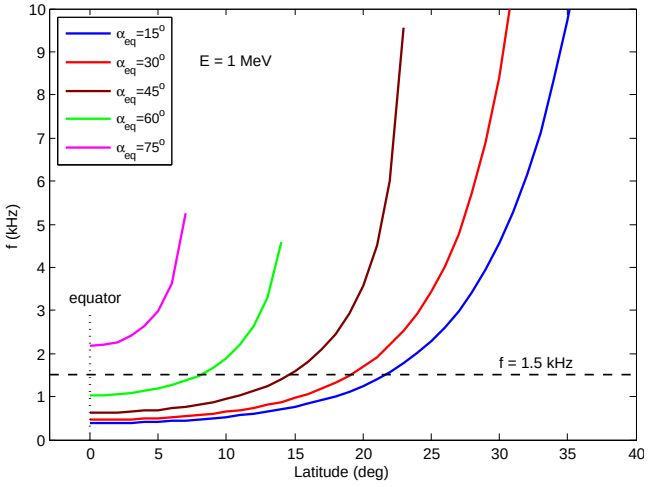

Figure 7. First-order resonant wave frequencies as a function of latitude along the bounce orbit of 1 MeV electron at $L = 3$, for the five indicated equatorial pitch angle (i.e., 15°, 30°, 45°, 60°, 75°). Here, the vertical dotted line shows the resonant wave frequencies for the five indicated equatorial pitch angle at the equator, while the horizontal dashed line shows the resonant latitude for the five indicated equatorial pitch angle when frequency is fixed as 1.5 kHz.

resonance harmonic. For $N = -1$ and 2, more test electrons undergo large variations in pitch angle and energy during resonant interactions with artificially generated 1 kHz whistler waves, consistent with the differences in local diffusion coefficients obtained based on test particle simulations.

In the calculations above, we have assumed a pitch angle of 30° and performed the test particle simulation at the equator. However, electron pitch angles can change in a wide range when they move along the ambient magnetic field line, and consequently the resonance can occur at any other latitudes besides the equator as long as the energy and pitch angle of the electron satisfy the resonant condition with the present wave. Figure 7 shows the first-order resonant wave frequencies as a function of latitude along the electron bounce trajectory at $L = 3$, for 1 MeV electrons at the five indicated equatorial pitch angles (i.e., 15°, 30°, 45°, 60°, and 75°). Shown as color-coded curves, resonant frequencies increase as the electron moves toward to higher latitudes. A sharp positive gradient occurs near the magnetic mirror latitudes – resulting from quickly increasing local pitch angle and magnetic field strength with latitude. Comparisons between the five curves also indicate that electrons with smaller equatorial pitch angles can resonate with waves in a broader frequency band from a few hundred Hz to above 10 kHz, as they can move to higher latitudes. In contrast, electrons with larger equatorial pitch angle resonate with waves only in a narrower frequency band. In addition, at a certain latitude, electrons with larger equatorial pitch angles resonate with higher-frequency whistler waves.

We now investigate the resonant interaction of artificial ELF/VLF waves with relativistic electrons (1 MeV) at various pitch angles. Runs of test particle simulation are set up in the same manner as for Fig. 5, but the frequency of generated whistler wave changes with initial pitch angle in order to satisfy the resonance conditions with 1 MeV electrons when we fix the resonant latitude at the equator (the resonant frequencies are indicated by the vertical dotted line in Fig. 7), or the resonant latitude changes with equatorial pitch angle when we fix the wave frequency as 1.5 kHz (the resonant latitudes are indicated by the horizontal dashed line in Fig. 7). The simulation results are presented in Figs. 8–10.

Figure 8 shows the model temporal variations of electron pitch angle (first row) and kinetic energy (third row) of 1 MeV electrons at the five initial pitch angles (i.e., 15°, 30°, 45°, 60°, and 75°), resulting from the first order resonance with artificial ELF/VLF waves at the equator of $L = 3$. Corresponding to the five initial pitch angles, the resonant wave frequencies that are used as input into the test particle simulation codes are 388.35 Hz, 460.35 Hz, 627.55 Hz, 1029.1 Hz, and 2170.0 Hz. As in Fig. 5, we present the wave-induced changes in pitch angle and energy of 15 randomly selected electrons, which again represent a stochastic profile in both domains. In principal, within 400 gyroperiods (~ 0.037 s), changes in electron pitch angle and kinetic energy are largest for 1 MeV electrons with an initial pitch angle of 15°, between $\pm 0.5°$ and between ± 0.1 keV,

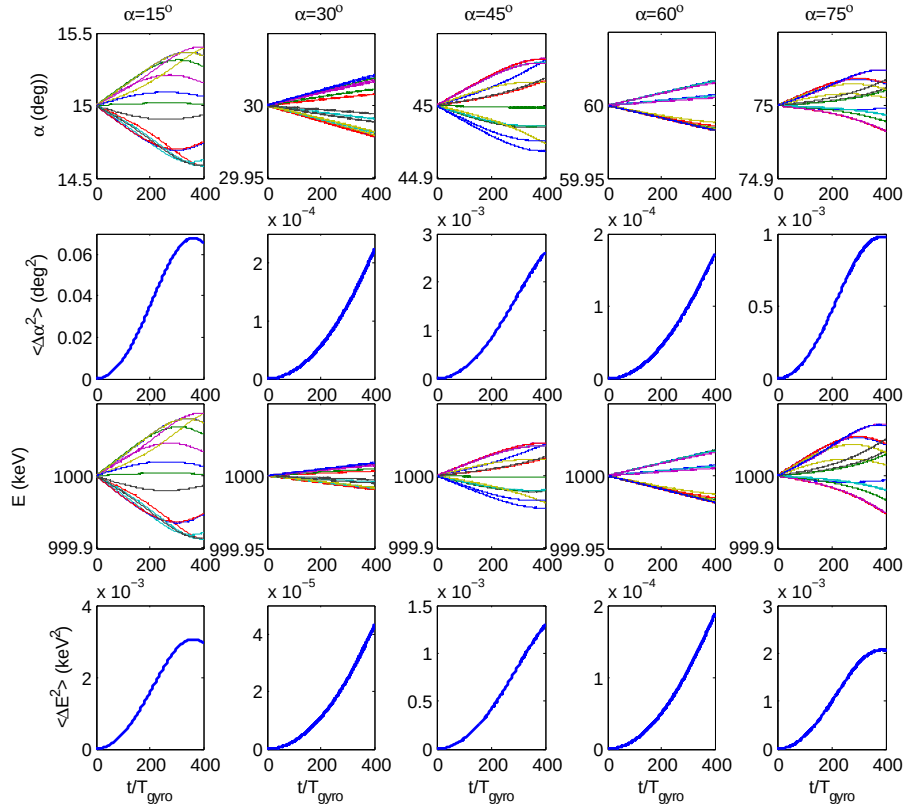

Figure 8. Results of resonant diffusion of 1 MeV electrons having five initial pitch angles, from left to right, 15°, 30°, 45°, 60°, and 75°, for the $N = 1$ resonance: changes of pitch angle (first row) and kinetic energy (third row) of 15 randomly selected electrons, and $\Delta\alpha^2$ (second row) and $\Delta \boldsymbol{E}^2$ (fourth row) averaged over all 200 electrons. The wave-normal angle is fixed as 100°, but the wave frequencies vary with initial electron pitch angle to satisfy the $N = 1$ resonance condition.

respectively. The temporal variations of $\left(\Delta\alpha^2, \Delta \boldsymbol{E}^2\right)$ averaged over all 200 test electrons are shown respectively in the second and fourth rows. The resonant timescales are about 400 gyroperiods for all five cases, and they show clear diffusion scattering in pitch angle and energy within the above time duration. The changes in electron pitch angle and kinetic energy, that is, $\left(\Delta\alpha^2, \Delta \boldsymbol{E}^2\right)$, are significantly initial pitch-angle dependent. Qualitatively, $\Delta\alpha^2$ and $\Delta \boldsymbol{E}^2$ are much larger at pitch angles of 15° and 45° than the other pitch angles.

To quantitatively evaluate the test particle diffusion rates and investigate its pitch-angle dependence, we perform the test particle simulation runs for a number of initial pitch angles from 5° to 80° in steps of 5° at the equator. Correspondingly, the wave frequency is carefully selected to initially satisfy the $N = 1$ resonance condition with 1 MeV electrons. The obtained profiles of $D_{\alpha\alpha}^{\mathrm{TP}}$ and $D_{\mathrm{pp}}^{\mathrm{TP}}$ (black curves) are presented in Fig. 9 as a function of initial pitch angle for 1 MeV electrons. These test particle simulation results show that (1) artificially generated single-frequency ELF/VLF waves can drive efficient local pitch-angle scattering of MeV electrons at a rate of $\sim 10^{-4}\,\mathrm{s}^{-1}$ at low-pitch angles near the loss cone at the equator; (2) in contrast, momentum diffusion by artificially generated single-frequency ELF/VLF waves is minor, mainly due to the large ambient electron density in the plasmasphere; and (3) $D_{\alpha\alpha}^{\mathrm{TP}}$ roughly decreases with pitch angle, while $D_{\mathrm{pp}}^{\mathrm{TP}}$ tends to exhibit much smaller pitch-angle dependence. The non-monotonic variations in the test particle diffusion rates may originate from the resonances with artificial whistler waves at different frequencies, which may change the values of $k_{//}$ and then affect the wave–particle interaction process.

In order to validate these test particle simulation results, we use the UCLA Full Diffusion Code (FDC) (Ni et al., 2008; Shprits and Ni, 2009) to compute the quasi-linear local diffusion coefficients at the magnetic equator for quantitative comparisons. The FDC outputs of local pitch-angle scattering rates and momentum diffusion coefficients are shown as red curves in Fig. 9. Since the quasi-linear formulation deals with broadband, continuous frequency spectrum, FDC requires a Gaussian frequency spectrum and a Gaussian wave-normal angle distribution as inputs. But the present test particle simulation approach focuses on monochromatic waves. To make the comparisons as meaningful as possible, we set

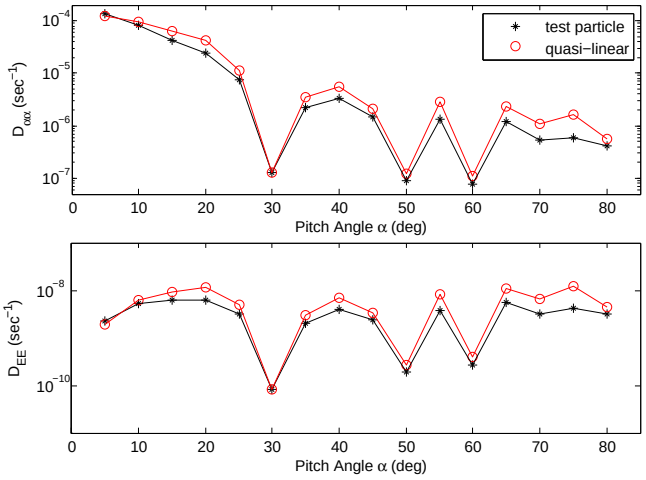

Figure 9. Comparisons of (top) pitch-angle diffusion rates and (bottom) momentum diffusion rates obtained from test particle simulations (blue curves) and quasi-linear formulation (red curve) for 1 Mev electrons at the equator. The wave-normal angle is fixed as 100°, and the wave frequencies vary with initial electron pitch angle to satisfy the $N = 1$ resonance condition at the equator.

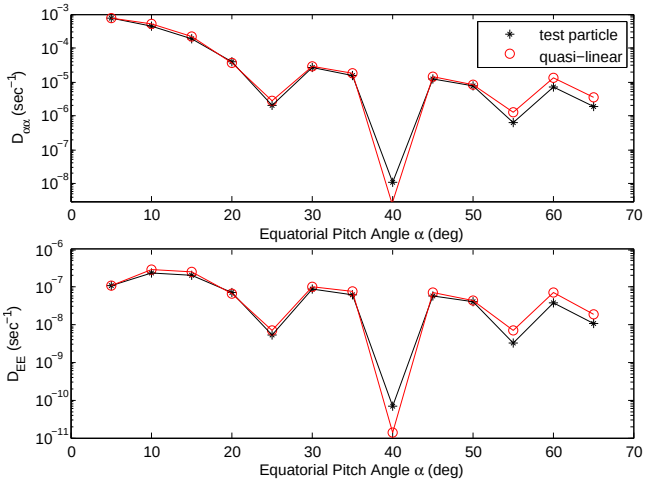

Figure 10. Same as Fig. 9, but the wave frequency is fixed as 1.5 kHz, and the resonant latitude vary with initial electron pitch angle to satisfy the $N = 1$ resonance condition.

up the wave spectrum with a half bandwidth of 0.1 Hz and centered at the resonant wave frequency corresponding to each considered pitch angle. The wave power is assumed to be distributed over the wave-normal angles of 79.5° to 80.5° and peak at 80° (the fixed wave-normal angle adopted for the test particle results in Fig. 9). For consistency, only the contribution of the $N = 1$ resonance is considered in the FDC evaluations. Despite certain difference in the absolute values, the results of local diffusion rates obtained based on two different methods (i.e., test particle simulations and quasi-linear formulation) agree well, showing identical trends of variation with respect to initial pitch angle and similar magnitudes of local scattering rates.

Figure 10 presents the profiles of $D_{\alpha\alpha}^{\mathrm{TP}}$ and $D_{\mathrm{pp}}^{\mathrm{TP}}$ (black curves) as a function of initial equatorial pitch angle for 1 MeV electrons that resonate with a 1.5 kHz wave at different latitudes. Note that the test particle simulations remain localized at the resonant latitudes and are performed in homogeneous background with the dipolar magnetic field strength at the resonant latitude. The equatorial pitch angles are set from 5° to 80° in steps of 5° but only those below 70° can undergo resonances with 1.5 kHz whistler waves at the considered latitudes (as shown in Fig. 7). We also use the UCLA FDC to compute the quasi-linear local diffusion coefficients for each equatorial pitch angle at the corresponding resonant latitude, which are shown as red curves to compare with our test particle simulation results.

Similar to Fig. 9, the results in Fig. 10 show intense local pitch-angle scattering and relatively weak momentum diffusion, which further confirms that pitch-angle scattering by artificially generated whistler-mode ELF/VLF waves can dominantly lead to the precipitation of high-energy electron in the plasmasphere. Furthermore, our test particle simulation results of local diffusion rates show good agreement with quasi-linear diffusion coefficients, which, together with Fig. 9, demonstrates the applicability of both methods to quantify the resonant diffusion effect of artificial generated ELF/VLF whistlers on high-energy plasmaspheric electrons.

5 Discussions

Since all test particle simulations in this study are performed around a certain latitude (i.e., localized), the wave-normal angle, the background magnetic field, and electron density are assumed as constant in each run for the sake of simplicity. As a matter of fact, bounce-averaging simulations in the inhomogeneous magnetic field such as a dipole field (Summers et al., 2007a, b; Tao et al., 2012) are more realistic, in which electron bounce back and forth along the magnetic field line and resonate with the single wave at certain latitudes. We caution that while our test particle simulation results (Figs. 9 and 10) show that artificially generated whistlers can induce efficient pitch-angle scattering near the loss cone, it is insufficient to suggest similarly intense electron-scattering loss when considering the bounce motion of the electron in an inhomogeneous magnetic field. The diffusion rates after bounce-averaging are expected to be smaller than the local values (e.g., Summers et al., 2007b), as single wave-induced resonance tends to occur at quite limited latitudes over the whole bounce period. Incorporating realistic magnetic field model into our test particle code will be the subject of our following studies to perform more accurate and comprehensive investigations on the processes of wave–particle resonant interactions and on the resonant diffusion effect by artificially generated ELF/VLF whistlers.

In the present study, we have introduced the term "resonance timescale" as the time duration within which the resonant interactions between artificially generated monotonic ELF/VLF waves and high-energy electrons can occur and drive cumulative variations in electron pitch angle and kinetic energy. The definition of resonance timescale is similar to that of resonance time introduced by Helliwell (1967), which was described as the time period when the electrons are fully bunched. For realistic magnetic field the "resonance timescale" is determined by the competition of wave field and magnetic field inhomogeneity (e.g., Shklayr and Matsumoto, 2009; Artemyev et al., 2013). Within the period of a resonance timescale, the variations of pitch angle and kinetic energy ($\Delta\alpha^2$ and $\Delta \boldsymbol{E}^2$) due to localized resonance are stochastic, which is consistent with the results of Tao et al. (2011). Actually, this stochastic feature can be captured by test particle simulations using either homogeneous or inhomogeneous magnetic field. However, for the present study, if the test particle simulation runs for enough time, the curves of $\Delta\alpha^2$ and $\Delta \boldsymbol{E}^2$ tend to show an oscillating profile in a Hamiltonian manner for the time period far exceeding the resonance timescale. We note that this periodicity of pitch angle and energy variation is due to the homogeneity of the chosen magnetic field. In addition, lack of nonlinear effects is another disadvantage of the chosen homogeneous magnetic field. Since magnetic field inhomogeneity can account for particle acceleration due to nonlinear interactions with waves (Bell, 1984; Shklayr and Matsumoto, 2009; Artemyev et al., 2012), our presented localized test particle simulations do not include the nonlinear effects, which also need a careful consideration by extending the model to inhomogeneous background magnetic field in future studies.

Despite the above aspects for improvements, by a combination of ray tracing technique and test particle simulation, this study is dedicated to calculation of the electron resonant diffusion driven by monotonic artificial ELF/VLF waves due to ionospheric modulation and shows intense localized wave-induced resonant scattering of energetic electrons in the plasmasphere. The results support the feasibility of artificial triggering of ELF/VLF whistler waves for removal of high-energy electrons within the plasmasphere at low-L shell. Moreover, our results show quantitatively good agreement with quasi-linear diffusion coefficients, confirming the applicability of both methods to evaluate the resonant diffusion effect of artificial generated ELF/VLF whistlers.

6 Conclusions

In this study we have simulated the ray path of ELF/VLF emissions in the inner magnetosphere by assuming that these waves at different frequencies are already generated by modulated HF heating of the ionosphere. Following the relativistic resonance condition, we have evaluated electron resonant energies along the artificially triggered whistler waves. Eventually, test particle simulations have been implemented to investigate the effects of resonant-scattering high-energy plasmaspheric electrons due to triggered ELF/VLF waves at $\sim$500 Hz–4 kHz under various conditions. The wave-induced rates of local pitch-angle scattering and momentum diffusion are also quantified, which show good agreement with the UCLA FDC quasi-linear diffusion coefficients. Our major conclusions are summarized as follows:

1. The spatial extent of L shell and magnetic latitude of ELF/VLF waves due to modulated HF heating of the ionosphere can be significantly controlled by generated wave frequency and the magnetic latitude where they are triggered initially. Ray tracing results also show that artificially triggered whistler waves are highly oblique in the magnetosphere. Along the ray path, artificially triggered ELF/VLF waves can resonate with electrons at energies from $\sim$100 keV to $\sim$10 MeV.

2. Changes in pitch angle and kinetic energy for a set of test electrons due to resonant interactions with single-frequency ELF/VLF waves are stochastic. Within the period of resonance timescale, the averages of $\Delta\alpha^2$ and $\Delta \boldsymbol{E}^2$ over all test electrons increase monotonically with time, and demonstrate reasonably linear profile for both cyclotron resonances and Landau resonance, the slopes of which, however, show a strong dependence on resonance harmonics.

3. Local pitch-angle scattering rates due to artificial, monotonic ELF/VLF whistlers $\sim$10 pT, obtained by test particle simulations, tend to be large near the loss cone, suggesting the feasibility of artificial triggering of ELF/VLF whistler waves for removal of high-energy plasmaspheric electrons. However, bounce-averaged diffusion should be more realistic, which will be an important extension of this study. In contrast, momentum diffusion of relativistic electrons is minor, mainly due to high-cold plasma density of the plasmasphere.

4. Our test particle simulation results of diffusion rates show good agreement with quasi-linear diffusion coefficients, demonstrating the applicability of both methods to quantify the resonant diffusion effect of artificial generated ELF/VLF whistlers on high-energy plasmaspheric electrons, which should be true since the triggered ELF/VLF emissions are generally weak and nonlinear effects are negligible.

Acknowledgements. This work is supported by the National Natural Science Foundation of China (NSFC) under the grant 41204120 and by the Fundamental Research Funds for the Central Universities under the grant 2042014kf0251. S. S. Chang especially thanks the sponsorship of the China Scholarship Council for one-year visiting program hosted at the Department of Atmospheric and Oceanic Sciences of University of California, Los Angeles.

Topical Editor I. A. Daglis thanks three anonymous referees for their help in evaluating this paper.

References

Abel, B. and Thorne, R. M.: Electron scattering loss in Earth's inner magnetosphere: 1. Dominant physical processes, J. Geophys. Res., 103, A22385, doi:10.1029/97JA02919, 1998a.

Abel, B. and Thorne, R. M.: Electron scattering loss in Earth's inner magnetosphere: 2. Sensitivity to model parameters, J. Geophys. Res., 103, A22397, doi:10.1029/97JA02920, 1998b.

Albert, J. M.: Analysis of quasi-linear diffusion coefficients, J. Geophys. Res., 104, A22429, doi:10.1029/1998JA900113, 1999.

Artemyev, A. V., Krasnoselskikh, V. V., Agapitov, O. V., Mourenas, D., and Rolland, G.: Non-diffusive resonant acceleration of electron in the radiation belts, Phys. Plasmas, 19, 122901, doi:10.1063/1.4769726, 2012.

Artemyev, A. V., Vasiliev, A. A., Mourenas, D., Agapitov, O. V., and Krasnoselskikh, V. V.: Nonlinear electron acceleration by oblique whistler waves: Landau resonance vs. cyclotron resonance, Phys. Plasmas, 20, 122901, doi:10.1063/1.4836595, 2013.

Barr, R. and Stubbe, P.: ELF radiation from the Tromsø "Super Heater" facility, Geophys. Res. Lett., 18, 1035–1038, 1991a.

Bell, T. F.: The nonlinear gyroresonance interaction between energetic electrons and coherent VLF waves propagating at an arbitrary angle with respect to the Earth's magnetic field, J. Geophys. Res., 89, 905–918, doi:10.1029/JA089iA02p00905, 1984.

Bell, T. F., Inan, U. S., Platino, M., Pickett, J. S., Kossey, P. A., and Kennedy, E. J.: CLUSTER observations of lower hybrid waves excited at high altitudes by electromagnetic whistler mode signals from the HAARP facility, Geophys. Res. Lett., 31, L06811, doi:10.1029/2003GL018855, 2004.

Bortnik, J.: Precipitation of Radiation Belt Electrons by Lightning-Generated Magnetospherically Reflecting Whistler Waves, Ph.D.'s thesis, Stanford University, California, 2005.

Bortnik, J. and Thorne, R. M.: Transit time scattering of energetic electrons due to equatorially confined magnetosonic waves, J. Geophys. Res., 115, A07213, doi:10.1029/2010JA015283, 2010.

Bortnik, J., Inan, U. S., and Bell, T. F.: Energy distribution and lifetime of magnetospherically reflecting whistlers in the plasmasphere, J. Geophys. Res., 108, 1199, doi:10.1029/2002JA009316, 2003.

Bortnik, J., Inan, U. S., and Bell, T. F.: Temporal signatures of radiation belt electron precipitation induced by lightning-generated MR whistler waves: 1. Methodology, J. Geophys. Res., 111, A02204, doi:10.1029/2005JA011182, 2006a.

Bortnik, J., Inan, U. S., and Bell, T. F.: Temporal signatures of radiation belt electron precipitation induced by lightning generated MR whistler waves. 2: Global signatures, J. Geophys. Res., 111, A02205, doi:10.1029/2005JA011398, 2006b.

Dysthe, K. B.: Some studies of triggered whistler emissions, J. Geophys. Res., 76, 6915–6931, doi:10.1029/JA076i028p06915, 1971.

Ferraro, A. J., Lee, H. S., Allshouse, R., Carroll, K., Tomko, A. A., Kelly, F. J., and Joiner, R. G.: VLF/ELF radiation from the ionospheric dynamo current system modulated by powerful HF signals, J. Atmos. Terr. Phys., 44, 1113–1122, doi:10.1016/0021-9169(82)90022-8, 1982.

Helliwell, R. A.: A theory of discrete VLF emissions from the magnetosphere, J. Geophys. Res., 72, 4773–4790, doi:10.1029/JZ072i019p04773, 1967.

Inan, U. S. and Bell, T. F.: The plasmapause as a VLF wave guide, J. Geophys. Res., 19, 2819–2827, doi:10.1029/JA082i019p02819, 1977.

Inan, U. S., Chang, H. C., and Hellwell, R. A.: Electron precipitation zones around major ground-based VLF signal Sources J. Geophys. Res., 89, 2891–2906, doi:10.1029/JA089iA05p02891, 1984.

Inan, U. S., Bell, T. F., Bortnik, J., and Albert, J. M.: Controlled precipitation of radiation belt electrons, J. Geophys. Res., 108, 1186, doi:10.1029/2002JA009580, 2003.

Inan, U. S., Golkowski, M., Carpenter, D. L., Reddell, N., Moore, R. C., Bell, T. F., Paschal, E., Kossey, P., Kennedy, E., and Meth, S. Z.: Multihop whistler-mode ELF/VLF signals and triggered emissions excited by the HAARP HF heater, Geophys. Res. Lett., 31, L24805, doi:10.1029/2004GL021647, 2004.

James, H. G., Dowden, R. L., Rietveld, P., Stubbe, P., and Kopka, H.: Simultaneous observations of ELF waves from an artificially modulated auroral electrojet in space and on the ground, J. Geophys. Res., 89, 1655–1666, 1984.

Kulkarni, P., Inan, U. S., Bell, T. F., and Bortnik, J.: Precipitation signatures of ground-based VLF transmitters, J. Geophys. Res., 113, A07214, doi:10.1029/2007JA012569, 2010.

Lyons, L. R: Electron diffusion driven by magnetospheric electrostatic waves, J. Geophys. Res., 79, A4575, doi:10.1029/JA079i004p00575, 1974.

Mourenas, D., Artemyev, A. V., Agapitov, O. V., and Krasnoselskikh, V.: Analytical estimates of electron quasi-linear diffusion by fast magnetosonic waves, J. Geophys. Res. Space Phys., 118, 3096–3112, doi:10.1002/jgra.50349, 2013.

Ni, B., Thorne, R. M., Shprits, Y. Y., and Bortnik, J.: Resonant scattering of plasma sheet electrons by whistlermode chorus: Contribution to diffuse auroral precipitation, Geophys. Res. Lett., 35, L11106, doi:10.1029/2008GL034032, 2008.

Ni, B., Bortnik, J., Thorne, R. M., Ma, Q., and Chen, L.: Resonant scattering and resultant pitch angle evolution of relativistic electrons by plasmaspheric hiss, J. Geophys. Res. Space Phys., 118, 7740–7751, doi:10.1002/2013JA019260, 2013.

Platino, M., Inan, U. S., Bell, T. F., Parrot, M., and Kennedy, E. J.: DEMETER observations of ELF waves injected with the HAARP HF transmitter, Geophys. Res. Lett., 33, L16101, doi:10.1029/2006GL026462, 2006.

Piddyachiy, D., Inan, U. S., Bell, T. F., Lehtinen, N. G., and Parrot, M.: DEMETER observations of an intense upgoing column of ELF/VLF radiation excited by the HAARP HF heater, J. Geophys. Res., 113, A10308, doi:10.1029/2008JA013208, 2008.

Shprits, Y. Y. and Ni, B.: Dependence of the quasi-linear scattering rates on the wave normal distribution of chorus waves, J. Geophys. Res., 114, A11205, doi:10.1029/2009JA014223, 2009.

Shprits, Y. Y., Runov, A., and Ni, B.: Gyro-resonant Scattering of Radiation Belt Electrons during the Solar Minimum by Fast Magnetosonic Waves, J. Geophys. Res., 118, 648–652, doi:10.1002/jgra.50108, 2013.

Shklayr, D. and Matsumoto, H.: Oblique whistler-mode waves in the inhomogeneous magnetospheric plasma: resonant interactions with energetic charged particles, Surv. Geophys., 30, 55–104, 2009.

Summers, D. and Ni, B.: Effects of latitudinal distributions of particle density and wave power on cyclotron resonant diffusion rates of radiation belt electrons, Earth Planet. Space, 60, 763–771, 2008.

Summers, D., Ni, B., and Meredith, N. P.: Timescales for radiation belt electron acceleration and loss due to resonant wave-particle interactions: 1. Theory, J. Geophys. Res., 112, A04206, doi:10.1029/2006JA011801, 2007a.

Summers, D., Ni, B., and Meredith, N. P.: Timescales for radiation belt electron acceleration and loss due to resonant wave-particle interactions: 2. Evaluation for VLF chorus, ELF hiss, and electromagnetic ion cyclotron waves, J. Geophys. Res., 112, A04207, doi:10.1029/2006JA011993, 2007b.

Tao, X. and Bortnik, J.: Nonlinear interactions between relativistic radiation belt electrons and oblique whistler mode waves, Nonlin. Processes Geophys., 17, 599–604, doi:10.5194/npg-17-599-2010, 2010.

Tao, X., Bortnik, J., Albert, J. M., Liu, K., and Thorne, R. M.: Comparison of quasilinear diffusion coefficients for parallel propagating whistler mode waves with test particle simulations, Geophys. Res. Lett., 38, L06105, doi:10.1029/2011GL046787, 2011.

Thorne, R. M.: Radiation belt dynamics: The importance of wave-particle interactionse importance of wave-particle interactions, Geophys. Res. Lett., 37, L22107, doi:10.1029/2010GL044990, 2010.

Zheng, Q., Zheng, Y., Fok, M.-C., and Lui, A.: Electron energy diffusion and advection due to non-linear electron-chorus wave interactions, J. Atmos. Sol.-Terr. Phys., 80, 152–160, 2012.

Zheng, Q., Fok, M.-C., Zheng, Y., and Lui, A.: Non-linear whistler mode wave effects on magnetospheric energetic electrons, J. Atmos. Sol.-Terr. Phys., 102, 8–16, 2013.